Synthesis of anthracene-conjugates of truncated antifreeze protein sequences. Effect of end-group and photo-controlled dimerization on ice recrystallisation inhibition activity

Ben Graham, [a] Alice E. R. Fayter [a] and Matthew I. Gibson [a,b]*

[a] Department of Chemistry, University of Warwick, Gibbet Hill Road, Coventry, CV4 7AL, UK;

[b] Warwick Medical School, University of Warwick, Gibbet Hill Road, Coventry, CV4 7AL, UK.

Abstract

Biomacromolecular antifreezes distinguish ice from water, function by binding to specific planes of ice and could have many applications from cryobiology to aerospace where ice is a problem. In biology, antifreeze protein (AFP) activity is regulated by protein expression levels *via* temperature and light regulated expression systems but in the laboratory (or applications) the antifreeze activity is 'always on' without any spatial nor temporal control and hence methods to enable this switching represent an exciting synthetic challenge. Introduction of abiotic functionality into short peptides (e.g. from solid phase synthesis) to enable switching is also desirable, rather than on full-length recombinant proteins. Here truncated peptide sequences based on the consensus repeat sequence from Type I AFPs (TAANAAAAAAA) were conjugated to an anthracene unit to explore their photo-controlled dimerization. Optimization of the synthesis to ensure solubility of the hydrophobic peptide included the addition of a dilysine solubilizing linker. It was shown that UV-light exposure triggered reversible dimerization of the AFP sequence, leading to an increase in molecular weight. Assessment of the ice recrystallization inhibition activity of the peptides before and after dimerization revealed only small effects on activity. However, it is reported here for the first time that addition of the anthracene unit to a 22 amino-acid truncated peptide significantly enhanced IRI compared to the free peptide, suggesting an accessible synthetic route to allow AFP activity using shorter, synthetically accessible, peptides with photo-reactive functionality.

Keywords

Antifreeze proteins, Photo-responsive, Ice Recrystallisation, Cryobiology,

Introduction

Antifreeze proteins (AFPs) are produced by a number of marine and insect species in cold habitats.[1–3] AFPs have the remarkable effect of restricting ice crystal growth,[2] allowing species like the right-eyed flounder to survive without freezing solid in icy waters. During the summer months, a gene circuit inhibits the synthesis of AFPs by the liver.[4] In application areas (e.g. medicine) there is no simple way to gain localised, spatiotemporal control over AFP function and there is a need to study the impact of chemical-modification on the AFP peptide to introduce additional functionality. Switchable activity would be particularly desirable in numerous fields, such as cryosurgery, (used for moles, warts, and benign/malignant melanomas[5]) for localised cold-protection. Cryotherapy finds use in the treatment of tumours and cancerous growths on organs such as the lungs, kidneys, and liver, where the sudden low temperature and ice crystal growth causes catastrophic cell damage and shutting off the tissues blood supply resulting in tissue ischemia. [5–7] However, extensive damage to surrounding healthy tissues in both cryosurgery and cryoablation is a problem.[8] Ice recrystallization inhibitors[9–12] have been shown to increased post thaw recovery and viability after cryopreservation of a range of cells such as blood,[13–16] islet cells,[17] stem cells[18] and various cell lines.[19–21]. However, it should be noted that antifreeze proteins can also cause increased cryo-damage depending on context and concentration; for example the formation of specular ice due to how AFPs bind ice crystals is actually destructive.[22] The ability to either restrict ice growth (to preserve surrounding tissue) or promote specular ice (to increase damage to targeted regions) would both ultimately alleviate post-surgery symptoms and improve patient compliance as well as providing a tool for fundamental studies on ice crystal growth kinetics. Therefore, there is potential to develop an ice recrystallisation inhibitor with spatio-temporal control over its activity through the addition of

photo-reactive units, and to evaluate the impact of these modifications on function. Light is a desirable trigger, as it has high spatial resolution and the wavelengths can be tuned to different triggers. Such photo triggers have found wide application in areas such as cell-laden hydrogels,[23,24] light triggered polymerization[25–27] and even to gain control over gene level expression.[28,29]

There are currently very few examples of stimuli-responsive control of IRI activity of AFPs, nor studies on the impact of abiotic functionality on the activity of AFPs. Ben and coworkers have developed azobenzene derived carbohydrate (fluoro)surfactants which showed moderate, but statistically significant photo-control of IRI.[30,31] Sonnischen *et al.* have demonstrated the use of azobenzene linkages to reversibly deform antifreeze proteins upon exposure to light, modulating their IRI activity.[32] Gibson and co-workers have used catechols to reversibly assemble polymeric IRIs through co-ordination of Fe^{3+} ions, leading to pseudo-star polymers with increased activity due to their increased molecular weight.[33] Other than these isolated examples, there are no other reports, to the best of our knowledge, of dynamically controllable IRIs. In contrast, there is vast literature on the use of photo-reactive units to control materials properties. Azobenzene has featured heavily in the literature as a biological photoswitch, and Woolley *et al.* have reviewed its deployment in this context.[34] Importantly, the ability to 'red-' or 'blue-shift' the photodimerization wavelengths of azobenzene's through aromatic functional group substitution is particularly important, allowing for application in sensitive biological systems where UV exposure would otherwise cause harm. Azobenzene has found use in the photocontrol of the helical conformations and solution structures of several proteins and DNA, and has been applied to controlling protein cross-linking, DNA transcription, and protein activity.[32,35,36] Azobenzene incorporation into peptides has also provided for the artificial introduction of a β-like turn in

normally α-helical structures through the application of a light stimulus.[34] This ability to order, and disorder, a protein was exploited by Aemissegger *et al.*, who demonstrated that the incorporation of an azobenzene motif could solicit the formation of a well-defined β-hairpin solution structure of a peptide when in the *trans* conformation, whilst the protein-photoswitch conjugate promoted peptide oligomerization when *cis*.[37] Furthermore, azobenzene derived tethered ligands have also been applied to the selective activation and deactivation of biological receptors and ion channels, such as nicotinic acetylcholine,[38] potentially providing a therapeutic effect.

Anthracene conjugates are another useful class of photo-triggers, as individual anthracene units are capable of 'dimerizing' *via* cycloaddition upon exposure to UV light. Some previous applications have included the incorporation of anthracene into DNA binding proteins,[39] increasing protein binding affinity when dimerized, whilst glycosylated anthracene derivatives have also shown promise as protein cleaving agents when irradiated.[40] Summerlin and co-workers have used anthracene to enable stimuli-induced changes in polymeric architecture.[41] Anthracene modified DNA has demonstrated dissimilar binding towards complementary DNA strands when dimerized, illustrating the potential role of DNA duplex formation in the control of a photochromic system.[42] Of particular interest is that upon photo-irradiation anthracene undergoes a [4+4] cycloaddition[43–45] resulting in a doubling of molecular weight, by bringing together two separate units. Antifreeze proteins,[46] and antifreeze glyco proteins[47] (as well as their mimics such as poly(vinyl alcohol)[48] show molecular weight dependent activity and hence anthracene offers a route to tune size and hence function.

Considering the above, this manuscript reports an investigation into the impact of incorporating the photo-responsive unit anthracene onto the chain ends of truncated antifreeze protein

sequences to evaluate the impact of end-group modifications on activity and the subsequent photo-dimerization. Truncated peptides from the consensus sequence of Type I antifreeze proteins are employed, and the conjugation to anthracene optimized. A range of characterization methods are employed to demonstrate successful conjugation of the anthracene and that photo-mediated dimerization can occur. The installation of an (IRI inactive) 11 – amino acid AFP-inspired sequence demonstrated no IRI activity in either the dimeric or monomeric forms. However, an otherwise similarly inactive 22 – amino acid sequence was shown to be IRI active upon the addition of the anthracene end group showing that addition of the photo-responsive units can bring additional activity also. After successful photo-mediated dimerization there was only a small change in activity between monomeric and dimeric forms. These results show that minimalistic AFPs sequences can be employed as IRIs by incorporating end-group functionality, which also brings the opportunities to modulate their properties by light.

Experimental Section

Materials

Fmoc-Lys-ε-(Boc)-OH, *N*-α-Boc-*L*-asparagine, L-asparagine tert-butyl ester hydrochloride were purchased from Fisher Scientific UK Limited (Loughborough, UK) and NH_3Cl-Lys-ε-(NHBoc)-OMe was purchased from Fluorochem Limited (Glossop, UK). Dichloromethane, EDCI, OxymaPure™, triethylamine, hydrochloric acid solution (12M), sodium chloride, sodium hydroxide, sodium hydrogen carbonate, sodium carbonate, magnesium sulphate, sodium sulphate, acetonitrile, mercaptoacetic acid, 25% sodium methoxide in methanol, methanol, acetone, hexane, 9-anthracene carboxylic acid, dimethyl formamide, dimethyl acetamide, diethyl ether, alanine, ethyl acetate, 4-nitrophenyl chloroformate, benzylamine, *N*-Boc-ethylenediamine, 1,4-dioxane, *N*-hydroxysuccinimide, Amberlyst IR120 resin (hydrogen form), DMAP, propargyl alcohol, sodium ascorbate, $CuSO_4$, tert-butanol, Amberlyst(R) A26 hydroxide form were purchased from Sigma Aldrich Co Ltd (Gillingham, UK). AFP_{11} and AFP_{22} were purchased from Peptide Protein Research Limited (Bishops Waltham, UK). Celite 545 was purchased from VWR Limited (Lutterworth, UK). PVAc was provided by Christopher Stubbs in the Gibson Group (University of Warwick, UK). All were used without further purification. Phosphate-buffered saline (PBS) solution was prepared using preformulated tablets in 200 mL of Milli-Q water (>18.2 Ω mean resistivity) to give [NaCl] = 0.138 M, [KCl] = 0.0027 M, and pH 7.4.

Antifreeze protein type I was provided by Dr. Muhammad Hasan, obtained by recombinant expression in *E.coli.* from *barfin plaice.*[49] Sequence: DTASDAAAAAAATAAAAAAAAATAKAAAEAAAATAAAAR, Mw: 3285.53 $g.mol^{-1}$

Physical and analytical methods

^{1}H and ^{13}C NMR Spectra (300 – 400 MHz and 75 – 100 MHz, respectively) were recorded using a Bruker DPX-300/400 Spectrometer under standard NMR conditions. Chemical shifts were recorded in ppm and referenced to solvent residual peaks, using MestReNova NMR Spectroscopy software.

ESI MS experiments were performed on an Agilent 6130B Single QUAD ESI-LC MS spectrometer in either positive or negative mode with an H_2O/MeOH (80:20) eluent feed, with samples dissolved in water, methanol or acetonitrile, unless otherwise stated.

Absorption UV/Vis (Ultra-violet/visible spectroscopy) spectra were acquired on an Agilent Technologies Cary 60 Variable Temperature UV-Vis spectrophotometer at room temperature fitted with Holographic Grating (27.5 × 35 mm, 1200 lines/mm, blaze angle 8.6° at 240 nm), a double beam, Czerny-Turner monochromator, 1.5 nm fixed spectral bandwidth, full spectrum Xenon pulse lamp single source, dual silicon diode detectors, quartz overcoated optics, non-measurement phase stepping wavelength drive, room light immunity. Analysis undertaken using Agilent CaryWin UV Scan software. All sample spectra were acquired in Hellma Analytics High Precision Quartz UV Cuvettes. Machine was zeroed and solvent background subtracted. Irradiation experiments were carried out in a Vilber Lourmat™ Biolink™ BLX UV Crosslinker (Vilber, Germany) containing 5 x 8 W tubes (365 nm).

HPLC experiments were conducted on an Agilent 1260 Infinity II LC System (Bioinert) fitted with a quaternary pump and C18 reverse phase column. Detection was carried out with the UV module, and the UV lamp set at 213 nm. All samples were dissolved in methanol with an

injection volume of 100 μL, flow rate of 1 ml/min, and gradient solvent system (Initial: 100% MeOH to 50:50% MeOH/H_2O), at room temperature, over a 30-minute run time.

Circular Dichroism experiments were conducted on a standard Jasco J-1500 CD Spectrometer utilising 1 mm quartz cuvettes containing 200 μL of appropriately diluted aqueous sample, with measurements taken in the 260 – 180 nm range at a voltage not exceeding 600. Solvent (water) backgrounds were subtracted.

Fluorescence measurements were made using a BioTek Synergy HT multi-detection microplate reader and Gen5 software (*BioTek* Instruments, Winooski, VT).

Dynamic light scattering was conducted using a NanoZs (Malvern Instruments, UK). Scattered light was detected at 173º and the observed count rates recorded. Hydrodynamic radii (where appropriate) were determined using the manufacturer's software. Diameters are an average of 3 measurements using at least 10 scans.

Wide-angle X-ray scattering (WAXS) experiments were performed using a Xenocs Xeuss 2.0 equipped with a micro-focus Cu K_α source collimated with Scatterless slits. The scattering was measured using a Pilatus 300k detector with a pixel size of 0.172 mm x 0.172 mm. The distance between the detector and the sample was calibrated using silver behenate ($AgC_{22}H_{43}O_2$), giving a value of 0.161(3) m. The detector was fixed at an angle of 36° giving a 2θ range of 18.5 to 47.5°. Samples were mounted in 1.0 mm quartz capillaries (Capillary Tube Supplies Ltd).

Synthetic Procedures

Synthesis of methyl *N*^{2}-(*N*^{2}-(((9*H*-fluoren-9-yl)methoxy)carbonyl)-*N*^{6}-(*tert*-butoxycarbonyl)-L-lysyl)-*N*^{6}-(*tert*-butoxycarbonyl)-L-lysinate (1)

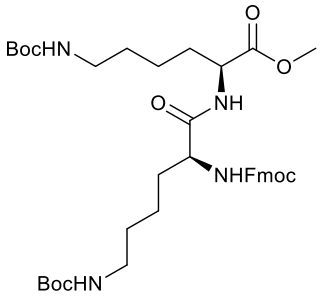

NHFmoc-Lys-ε-(NHBoc)-OH (0.5 g, 1.07 mmol) was dissolved in DCM (20 mL) with stirring, to which EDCI (0.246 g, 1.2 eqv, 1.28 mmol), OxymaPure™ (0.182 mg, 1.2 eqv, 1.28 mmol), and TEA (0.18 mL, 1.2 eqv, 1.28 mmol) were added. NH_3Cl-Lys-ε-(NHBoc)-OMe (0.348 g, 1.1 eqv, 1.17 mmol) was subsequently added, and the reaction mixture stirred at RT for 18 hours. The crude mix was subsequently extracted with dilute hydrochloric acid solution (x2 , 25 mL, pH 5 – 6), then saturated sodium hydrogen carbonate solution (x2, 30 mL), and finally brine (x1, 30 mL). The organic phase was dried over $MgSO_4$, filtered, and condensed *in vacuo*. The white solid was then crystallized from diethyl ether (30 mL), washed, filtered, and condensed *in vacuo*, yielding a colorless solid. 520 mg (68.6%). ^{1}H NMR (400 MHz, $CDCl_3$) δ = 7.82 – 7.21 (m, 8H), 6.82 (s, 1H), 5.71 (s, 1H), 4.75 (s, 2H), 4.56 (s, 1H), 4.38 (d, J = 5.7 Hz, 2H), 4.21 (t, J = 6.7 Hz, 2H), 3.73 (s, 3H), 3.22 – 2.98 (m, 4H), 1.86 (s, 2H), 1.71 (s, 2H), 1.58 – 1.24 (m, 26H). ^{13}C NMR (100 MHz, $CDCl_3$) δ = 172.71 (MeOC=O), 171.89 (NHC=O), 156.32 (2 x Boc C=O + Fmoc NHC=O), 143.95 (Fmoc), 141.37 (Fmoc), 127.83 (Fmoc), 127.21 (Fmoc), 125.22 (Fmoc),

120.08 (Fmoc), 79.27 (C-tert) 67.27 (COC=ONH), 54.73 (alpha-C), 52.53 (OMe), 52.21 (alpha-C), 47.21 (CH-Pent-Fmoc), 40.05, 32.23, 31.59, 29.56, 29.51, 28.54 (6 x CH_3), 22.52, 22.37. m/z (ESI, +ve) Expected 733.4, Observed 733.5 [100%, Na^+].

Synthesis of methyl *N*^{6}-(*tert*-butoxycarbonyl)-*N*^{2}-(*N*^{6}-(*tert*-butoxycarbonyl)-L-lysyl)-L-lysinate (2)

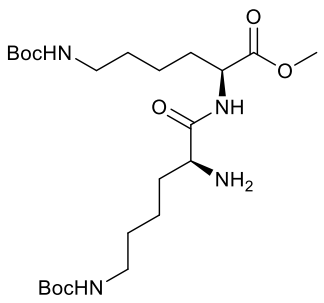

1 (1.4 g, 1.97 mmol) was dissolved in acetonitrile (10 mL), whilst mercaptoacetic acid (700 µL, 0.928 g, 10.07 mmol, 5.1 eqv) was added dropwise to a 25% solution of sodium methoxide in methanol (900 µL, 0.852 g, 15.76 mmol, 8 eqv) at 0ºC. To this pre-stirred solution, the solution of **1** in acetonitrile was added, and the combined mixture stirred for 12 hours, with heating at 50ºC. The mixture was then acidified to pH 5 – 6 with hydrochloric acid solution (1M) added dropwise, and the precipitated salts were filtered. The filtrate was subsequently condensed *in vacuo*, redissolved in methanol (5 mL), and the mercaptoacetic acid-dibenzofulvene by-product precipitated from water (20 mL). The milky-mixture was then filtered through a pad of Celite with water eluent, and the filtrate condensed *in vacuo*. Isolation of **2** followed through dissolution of the dry filtrate in acetone (10 mL) and then precipitation from hexane (30 mL), giving an off-white solid. 350 mg (36.4%). m/z (ESI, +ve) Expected 511.3, Observed 511.4

[100%, Na^+]. ^1H NMR (300 MHz, CH_3OH+D_2O) δ = 4.18 (t, J = 6.7 Hz, 1H), 3.82 (s, 1H), 3.55 (s, 3H), 2.90 – 2.77 (m, 4H), 2.02 (d, J = 2.4 Hz, 1H), 1.77 – 1.52 (m, 4H), 1.35 – 1.09 (m, 26H). ^{13}C NMR (101 MHz, MeOD) δ = 173.76 (MeOC=O), 173.16 (NHC=O), 158.51 (2 x Boc C=O), 128.50, 127.96, 126.12, 120.72, 79.82 (C-tert), 58.29, 55.94, 54.68, 53.28, 52.79 (OMe), 41.01, 34.91, 33.63, 31.97, 30.60, 30.44, 28.79 (6 x CH_3), 24.12, 23.12, 18.38.

Synthesis of methyl *N*^{2}-(*N*^{2}-(anthracene-9-carbonyl)-*N*^{6}-(*tert*-butoxycarbonyl)-L-lysyl)-*N*^{6}-(*tert*-butoxycarbonyl)-L-lysinate (3)

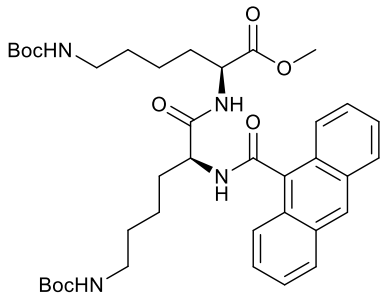

Anthracene-9-carboxylic acid (356 mg, 1.60 mmol, 2.2 eqv) was dissolved in DMF (30 mL) with stirring, and EDCI (154 mg, 0.86 mmol, 1.2 eqv), OxymaPure™ (114 mg, 0.86 mmol, 1.2 eqv), and TEA (112 µL, 0.86 mmol, 1.2 eqv) were added. **2** (350 mg, 0.72 mmol) was subsequently added, and the reaction mixture stirred at RT for 18 hours. The crude mix was then condensed to low volume *in vacuo* (~ 5 mL) and diluted with chloroform (30 mL), before being extracted with dilute hydrochloric acid solution (x2 , 25 mL, pH 5 – 6), then saturated sodium hydrogen carbonate solution (x2, 30 mL), and finally brine (x1, 30 mL). The organic phase was then re-acidified to pH 5 – 6 with hydrochloric acid solution (1M) and a column was packed with pre-rinsed Amberlyst beads (A26 hydroxide form). The acidified mix was then poured through the

column, eluting and washing with THF (3 x 10 mL). The collected eluent was then dried over $MgSO_4$, filtered, and condensed *in vacuo*, yielding an orange oil. 140 mg (28.2%). m/z (ESI, –ve) Expected 691.4, Observed 691.4 [100%, M-H^+]. ^{1}H NMR (400 MHz, $CDCl_3$) δ = 8.52 (s, 1H), 8.09 – 7.11 (m, 9H), 5.09 – 4.74 (m, 1H), 4.43 (m, 1H), 4.23 – 3.88 (m, 1H), 3.40 (s, 3H), 3.23 – 2.97 (m, 5H), 2.11 – 1.58 (m, 9H), 1.55 – 0.76 (m, 26H). ^{13}C NMR (101 MHz, $CDCl_3$) δ = 174.54 (MeOC=O), 168.62 (NHC=O), 156.25 (2 x Boc C=O), 154.32 (Anthracene NHC=O), 135.56 – 119.72 (Anthracene), 79.07 (C-tert), 57.43, 56.87, 56.49 – 55.84, 54.79, 52.35 (OMe), 50.32, 46.71, 45.63 – 45.14, 42.30, 41.17, 40.60, 40.02, 39.11, 37.34, 35.60, 35.25, 34.06, 33.82, 33.62, 33.47, 32.46, 29.80, 28.45 (6 x CH_3), 27.61, 27.42, 26.64, 26.26, 25.16, 22.60, 22.00, 15.66, 15.43, 15.21, 14.89, 14.23, 13.43.

Synthesis of methyl *N*^{2}-(*N*^{2}-(anthracene-9-carbonyl)-*N*^{6}-(*tert*-butoxycarbonyl)-L-lysyl)-*N*^{6}-(*tert*-butoxycarbonyl)-L-lysine (4)

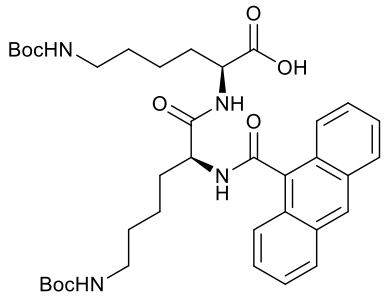

3 (140 mg, 0.20 mmol) was dissolved in methanol/water (1:1, 20 mL) and a large excess of sodium hydroxide added (500 mg, 62.5 eqv), and the mixture stirred at RT for 18 hours. The mixture was then acidified with hydrochloric acid solution (1M), dropwise, until pH 5 – 6. The mixture was then condensed *in vacuo*, and the product precipitated and isolated from acetone, giving a pale yellow solid. 100 mg (73.7%). m/z (ESI, -ve) Expected 677.4, Observed 677.3 [100%, M-H^+]. ^{1}H NMR (300 MHz, $CDCl_3$) δ = d 8.42 – 7.00 (m, 9H), 5.22 (s, 1H), 4.84 (s,

2H), 4.59 – 3.92 (m, 4H), 3.83 (s, 1H), 3.68 – 3.51 (m, 1H), 3.12 – 2.81 (m, 5H), 2.65 (d, J = 5.5 Hz, 1H), 1.97 – 1.52 (m, 4H), 1.52 – 1.11 (m, 29H). ^{13}C NMR (75 MHz, $CDCl_3$) δ = 173.95 (NHC=O), 157.74 (2 x Boc C=O), 156.89 (Anthracene NHC=O), 135.71 – 125.24 (Anthracene), 79.16 (C-tert), 69.76, 69.12, 55.38, 42.92, 39.07, 37.59, 36.06, 34.41, 33.85, 29.73, 28.54 (6 x CH_3), 23.82, 14.28, 13.52.

Representative / Optimized Procedure for Conjugative Coupling

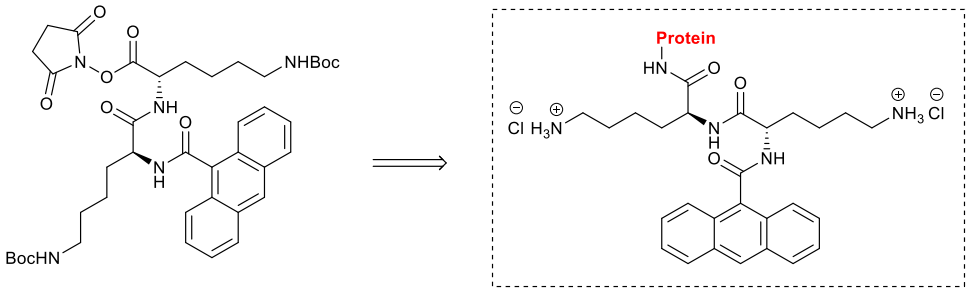

4 (30 mg, 0.044 mmol) was dissolved in dry DMF or DMAc and DCM (1:1, 5 mL) under a flow of dry nitrogen, and EDCI (17 mg, 2 eqv, 0.088 mmol) added, followed by *N*-hydroxysuccinimide (10 mg, 2 eqv, 0.088 mmol). The mixture was allowed to stir for 30 minutes to allow for the formation of **5** *in-situ*. Then, the antifreeze protein (AFP-22•TFA, 5 mg) or other species for conjugation was dissolved up in dry DMF or DMAc (2.5 mL) under a flow of dry nitrogen, and injected into the main flask, followed by a large excess of TEA (100 µL). The flask was then stirred for 4 days under dry nitrogen, with heating at 50ºC. The flask was subsequently cooled, exposed to air, and a large excess of sodium methoxide/methanol solution added (2 mL) – giving pH 12 and a fluorescent pink color change, and then stirred for 1 hour. After which, the flask was acidified to pH 1 with HCl (6M), resulting in decolorization, and stirred for 1 further hour. After the removal of the protecting/end groups, the mixtures were then diluted with

methanol (3 mL) and water (50 mL) and dialysed against water for 3 days (1 kDa dialysis tubing), with regular water changes. Upon completion, sedimentation was apparent, and the dialysis bags continued to fluoresce under long wave ultraviolet light, indicating the presence of a conjugated/large molecular weight anthracene unit within the bag. Both species were then reacidified to pH 2 with HCl (6M) and condensed *in vacuo* to give the final photoconjugate products, **6b** (AFP-22, 5.7 mg) and **9** (PVA, 12.5 mg). The initial candidates **6a** (AFP-11, 1 mg) and **6c** (Ala_8, 3.5 mg) were similarly prepared, but through a modified procedure. Mass Spectrometry of **6c** (as the Di-ε-Lys-Fmoc protected derivative) indicated a single peak present at 1613.8 m/z (100%), corresponding to the [Conjugate Mass + $Cl^{\bullet}$ – H^{+}].

Results and Discussion

A synthetic route to the peptide-anthracene (photo-responsive unit) conjugate in the 9- position was devised (Figure 1), restricting the total number of possible photodimers to 2 and favoring the *head-to-tail (ht)* isomer, due to the steric hindrance of the protein chains avoiding *head-to-head (hh)*. Truncated 11 or 22-residue peptides (termed AFP_{11} and AFP_{22} from this point) based on the consensus repeat sequence of a Type I AFP were obtained from (commercial) solid phase peptide synthesis; TAANAAAAAAA.[46] A dilysine linker was devised to be added between the anthracene and AFP to ensure that the conjugates produced were water soluble, especially considering the hydrophobicity of the alanine-rich AFP and anthracenes. Due to the presence of lysine in the variable positions of some AFP Type I strains (*TAA*AAAAAAA),[46] it was hypothesized that adding this di-amino acid lysine linker before the protein would be a tolerated modification. This would also act to prevent the steric bulk of the anthracene rings hindering the threonine residue which is essential for AFP activity,[2,50] or even in self-assembled peptide mimics.[51]

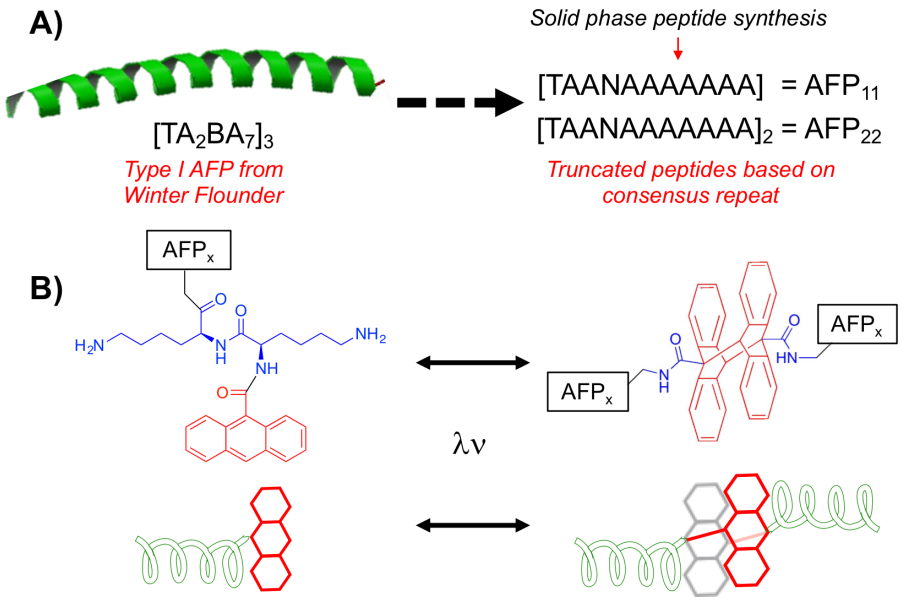

Figure 1. Proposed truncation and photo-dimerization strategy. A) Amino acid sequence truncation; B) Overall strategy to modulate AFP size *via* photo-dimerization of anthracene end-groups. Amino acid codes; A = alanine, T = threonine, N = asparagine. B indicates variable position.

The anthracene-dilysine unit was synthesized as shown in Scheme 1. Condensation coupling between two orthogonally protected lysine units using 1-ethyl-3-(3-dimethylaminopropyl)carbodiimide (EDCI) and OxymaPure™ gave the dipeptide **1** in good yield (68%). Subsequent removal of the Fmoc protecting group in the presence of a methyl ester to give intermediate **2** was performed with mercaptoacetic acid and sodium methoxide, with the mercaptoacetic acid scavenging the dibenzofulvene (DBF) by-product. The anthracene motif was then installed under similar EDCI/Oxyma coupling conditions and the methyl ester cleaved with hydroxide to give **4**. Due to the presence of *N*-Boc protecting groups on the lysine side chains, and the lone free amine in the antifreeze peptide stretch, **4** was suitable for direct EDCI/NHS

coupling to the *N*-terminus of the peptides, before *N*-Boc protecting group removal after AFP conjugation.

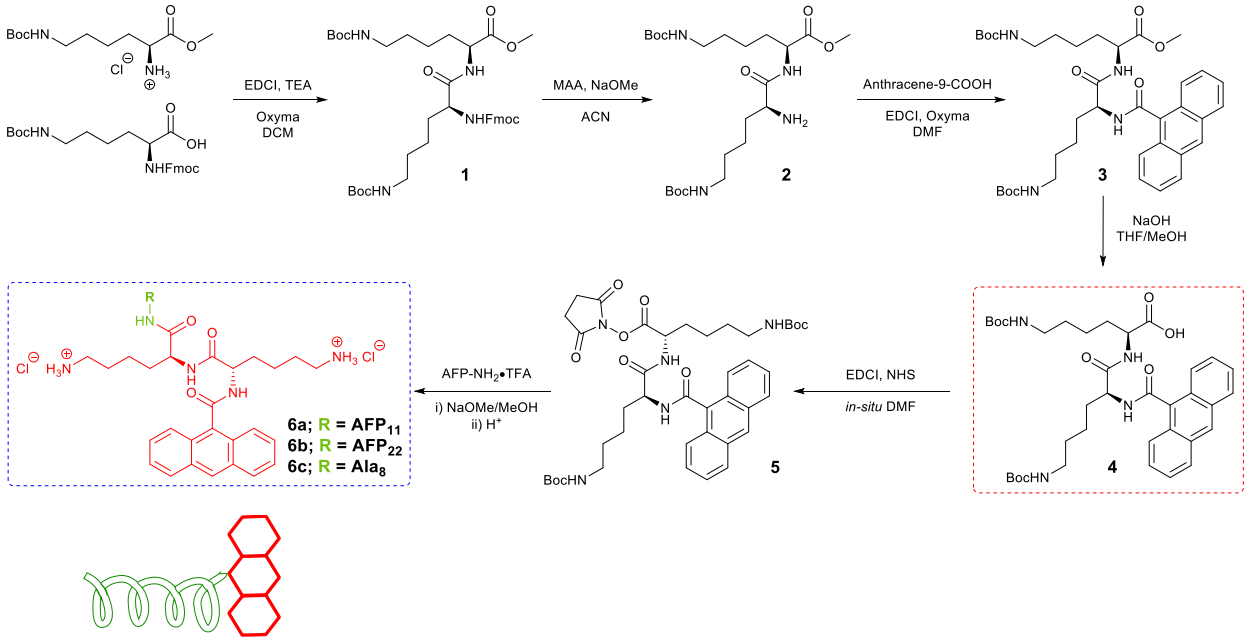

Scheme 1. Optimized synthetic route for the synthesis of the anthracene-photoconjugates. EDCI - 1-Ethyl-3-(3-dimethylaminopropyl)carbodiimide. TEA – Triethylamine. MAA – Mercaptoacetic acid. ACN – Acetonitrile. DMF – Dimethyl formamide. THF – Tetrahydrofuran. NHS – *N*-Hydroxysuccinimide. AFP-Antifreeze peptide. TFA – Trifluoroacetic acid.

Prior to conjugating the antifreeze protein to the photoresponsive unit, **4**, it was necessary to estimate the overall solubility of the AFP-photoconjugate. AFP Type I is > 70 % alanine and hence has low overall solubility and model compounds were necessary to ensure that the lysine linkers provided the needed solubility. Oligo-alanine was obtained by the *in situ* ring opening polymerization of L-alanine *N*-carboxy anhydride (NCA). To enable NCA formation, the method of Endo *et al.*[52] was used whereby the carboxylic acid was activated by functionalization with *para*-nitrophenyl chloroformate. Subsequent addition of benzyl amine (as the initiator) led to the

formation of the NCA, inducing ring opening polymerization. Poly(alanine) was obtained with a Mn_{SEC} of 790 g.mol^{-1} and dispersity of 1.1 Đ, of approximately 8 repeat units. This molecular weight was close to that of AFP_{11} and hence was suitable for initial studies. Scheme 2. Note, the low dispersity was of purified isolated oligoalanine, and the purification contributed to this fractionation.

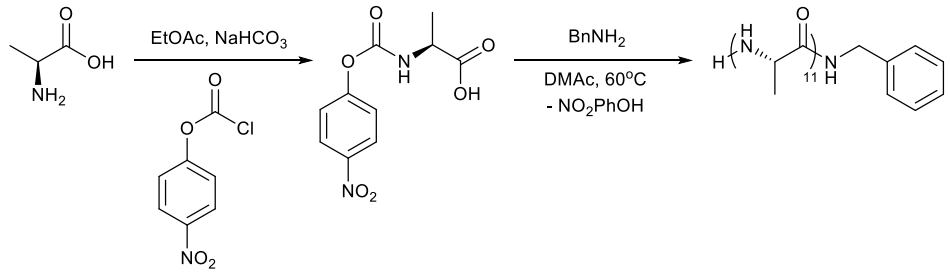

Scheme 2. Synthesis of poly(alanine) *via in-situ N*-carboxyanhydride ring opening polymerization. DMAc – Dimethyl acetamide. $BnNH_2$ – Benzylamine. NO_2PhOH – 4-Nitrophenol.

Attachment of the poly(alanine) stretch to **4** was achieved by condensation coupling, and when deprotected, was soluble in aqueous solution at a concentration of 3.5 mg.mL^{-1}. This indicated that the similarly hydrophobic and alanine rich antifreeze peptides would likely have reasonable solubility when conjugated. However, the conjugate visibly aggregated in phosphate buffered saline, demonstrating higher solubility when in saline alone (0.137 M NaCl), and hence saline was used for all subsequent IRI activity studies. It is crucial to note that saline is essential in the assays used later, and its omission can lead to false positives.[10,53]

Attachment of the truncated antifreeze proteins (AFP_{11} or AFP_{22}) to **4** was then performed, by the preparation of the *N*-hydroxysuccinimide ester, followed by NHS displacement by the *N*-terminus of the peptides. Due to the presence of threonine in the AFP peptide stretch, subsequent

hydrolysis by sodium methoxide followed, as despite the low reactivity of threonine's α-alcohol group, it was necessary to ensure that it had not formed any unwanted ester linkages. The *Boc* groups were subsequently removed with hydrochloric acid to give the final products (**6a; AFP_{11} / 6b; AFP_{22}**) as the dihydrochloride salt, which were dialysed to remove low molecular weight contaminants, reacidified, and isolated as a solid salt. Mass spectrometry of conjugate **6b** (hereafter referred to as PC-AFP_{22}) indicated an absence of unconjugated peptide (which possesses a high molecular weight, above the MWCO of the dialysis tubing), therefore indicating complete conversion. With these anthracene conjugates to hand, their photo-responsive behavior could be explored. Figure 2 shows the UV-Vis absorption spectra of the unconjugated anthracene-dilysine dihydrochloride salt in both water and methanol.

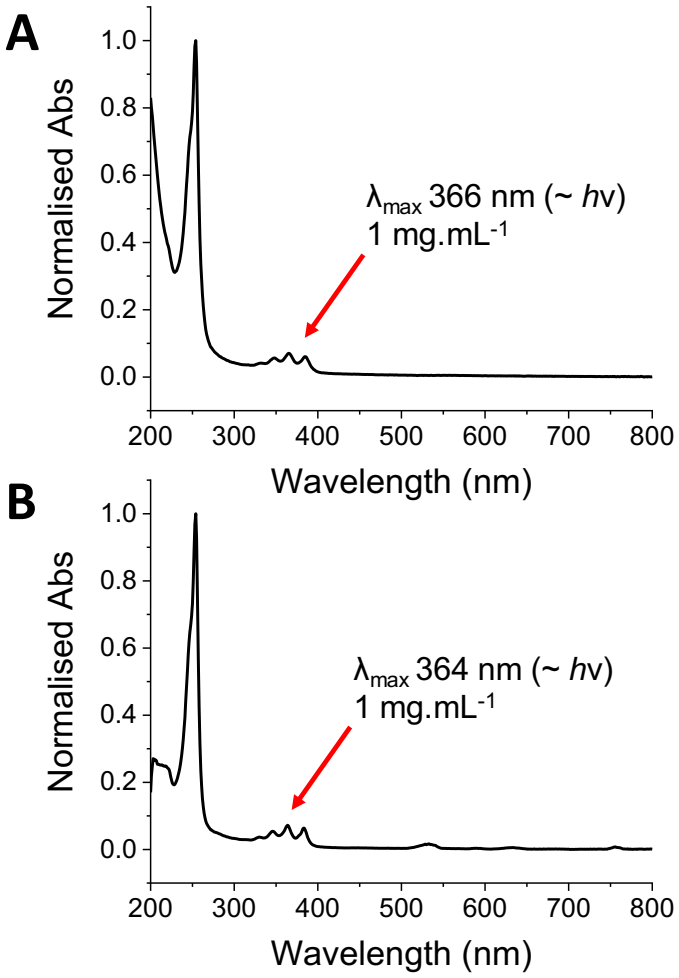

Figure 2. UV-Vis Spectra of unconjugated anthracene-dilysine dihydrochloride in A) H_2O and B) MeOH.

The UV-Vis showed the expected anthracene multiplet in the 340 – 390 nm region, with $\lambda_{max} \approx$ 365 nm, in both H_2O and MeOH. In order to establish the extent of dimerization upon irradiation and ensure complete formation of the photoproduct, UV exposure trials were then conducted. The anthracene-dilysine-poly(alanine) photoconjugate, **6c**, hereafter referred to as PC-Ala, was initially used to trial the photo dimerization processes, as shown in Figure 3.

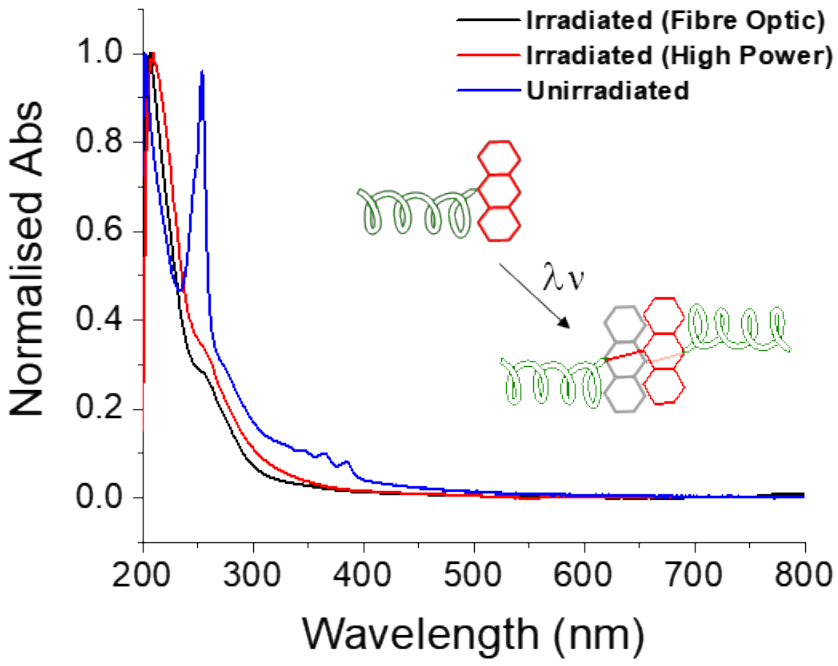

Figure 3. UV-Visible spectra showing effect of photo-irradiation, and dimerization, on PC-Ala.

After 24 hour exposure of PC-Ala, in aqueous solution, to both a high powered UV cross-linker and a fibre optic UV lamp (both at 365 nm), a complete loss of the multiplet in addition to the loss of the satellite peak at 255 nm was observed. This is consistent with cycloaddition induced dimerization of the anthracene motifs and provided proof of principle that the peptide conjugation does not inhibit this process due to steric hindrance.

The AFP-derived candidates; **6a** (PC-AFP$_{11}$) and **6b** (PC-AFP$_{22}$) were subsequently irradiated in pure water under UV 365 nm light, and after 1 hour, complete conversion to the dimerised product was observed by UV-Vis Spectroscopy, Figure 4. Complete loss of the triplet was again observed, in conjunction with a shift in the satellite peak. Importantly, when irradiated, no visible solution change occurred – ruling out inadvertent precipitation of the photo product dimer, which would otherwise impact upon concentration.

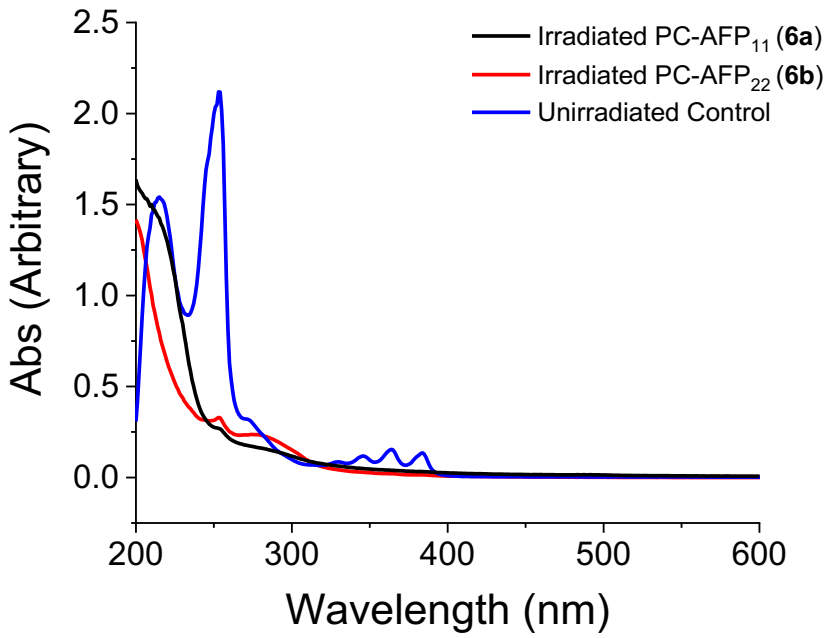

Figure 4. UV-Visible spectra of the Anthracene-AFP photoconjugates upon photo-irradiation.

Fluorescence analysis of the PC-AFP_{22} species showed a 72 % decrease in 360/40 nm emission post irradiation, providing additional evidence of successful dimerization. Mass spectrometry monitoring of the photo-dimerization process showed complete removal of the monomeric units, but no peaks associated with the dimer products were observed. Therefore, HPLC (high performance liquid chromatography) was used. HPLC analysis of the PC-AFP_{22} in its dimerized state relative to an undimerized 9-ACA control, Figure 5, indicated the presence of the dimeric form only (with small amount of aggregation also), as corroborated by literature confirming that a photo-driven process can be used to control the size of the AFP conjugates.[54,55]

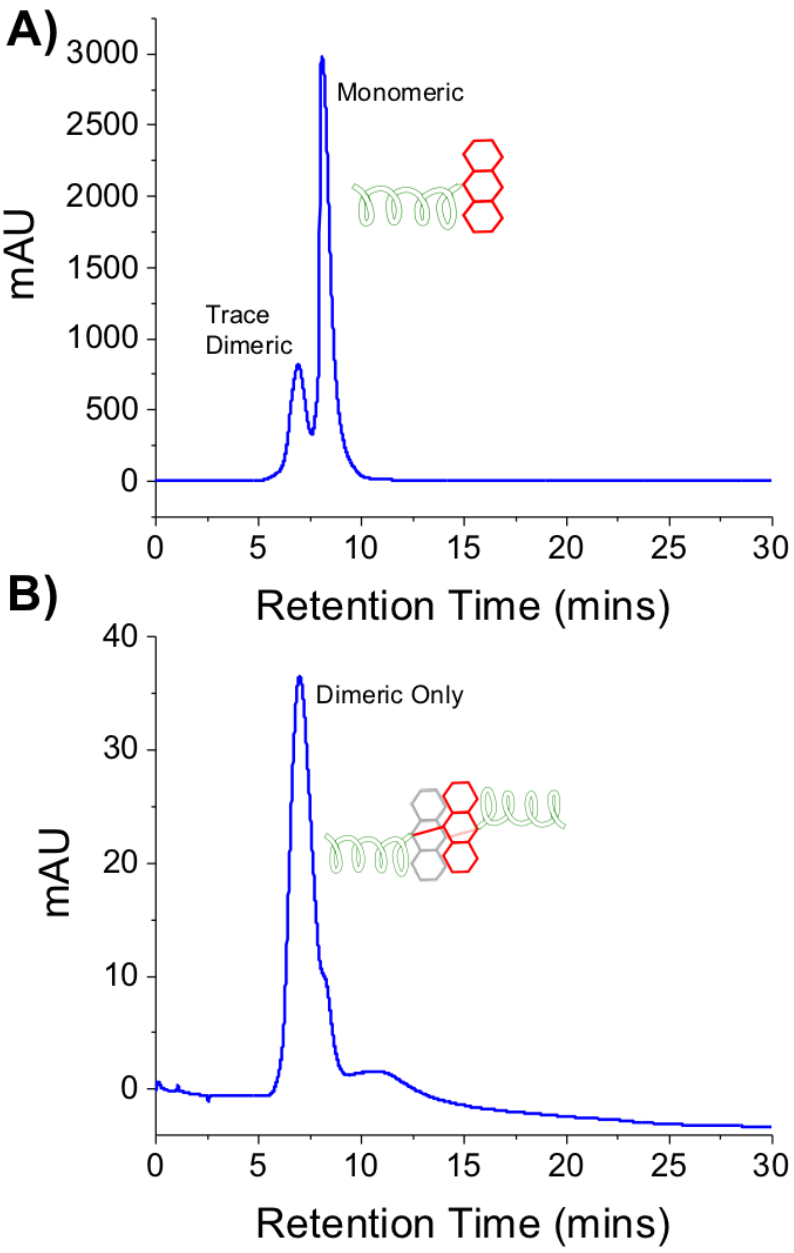

Figure 5. HPLC chromatograms of A) 9-ACA Control; B) PC-AFP$_{22}$ (**6b**) Dimer.

Circular dichroism (CD) spectroscopy, Figure 6, was employed to further investigate the dimerization process. AFP$_{11}$ showed a small degree of β-sheet character, as suggested by fitting analysis (ESI) and corroborated by literature,[56] as would be expected for a short alanine-rich stretch. AFP$_{22}$ was closer in nature to an α-helix (peak at 222 nm) which is seen for full length

Type I AFP. These differences in secondary structure are crucial to understanding the observed IRI activity (discussed below). When conjugated to the anthracene-dilysine, the PC-AFP$_{22}$ monomer had similar features to the free peptide but showed slight shifting and a stronger inclination in the second band at ~ 235 nm, implying some deviation in the secondary structure as a result of the attachment of the anthracene unit. This is possibly a result of helical seeding by the lysine residues and/or contributions from the aromatics in the 190 – 200 nm region. When irradiated with UV light (to induce dimerization), the same PC-AFP$_{22}$ dimer had a weaker CD signature, retaining a slight inclination of its former (unirradiated) signal morphology. Given the system possesses a central chromophore which is geometrically achiral, it is possible that it only has a small electronic chirality arising from coupling with the peptide chromophores, as a result, the induced CD could be expected to be comparatively small – further corroborating dimerisation.[57]

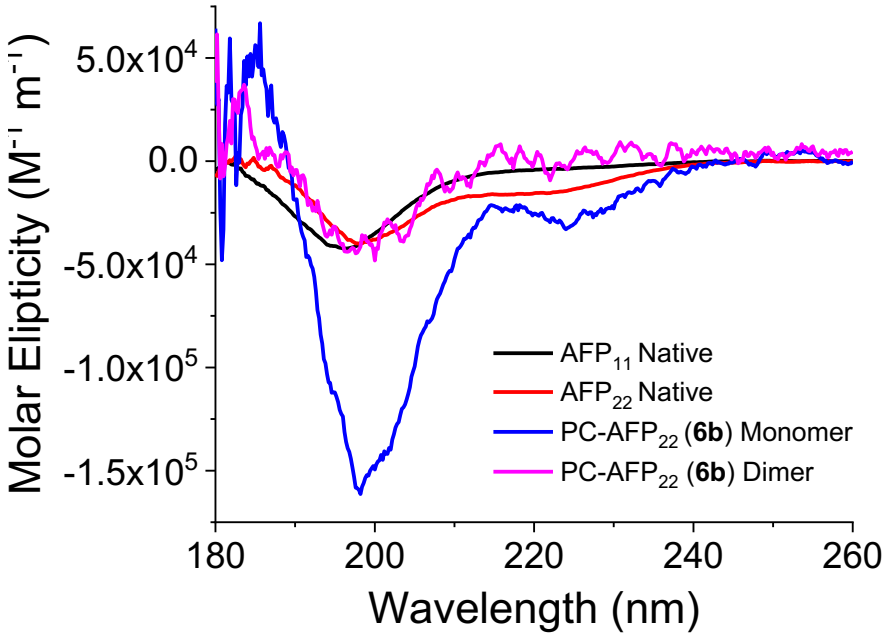

Figure 6. Circular dichroism spectra of anthracene-AFP conjugates and free peptides.

With the photo-controlled dimerization process confirmed, the peptides could be evaluated for their IRI activity. IRI activity was determined by the 'splat' assay, whereby a polynucleated ice wafer is annealed at – 8 °C, and the average crystal size determined after 30 minutes. The assay enables separation of nucleation from growth, and data is reported as the mean grain size (MGS) relative to the saline control [Note – saline not PBS was needed for peptides for solubility, as discussed above]. Smaller crystal sizes indicate greater activity.

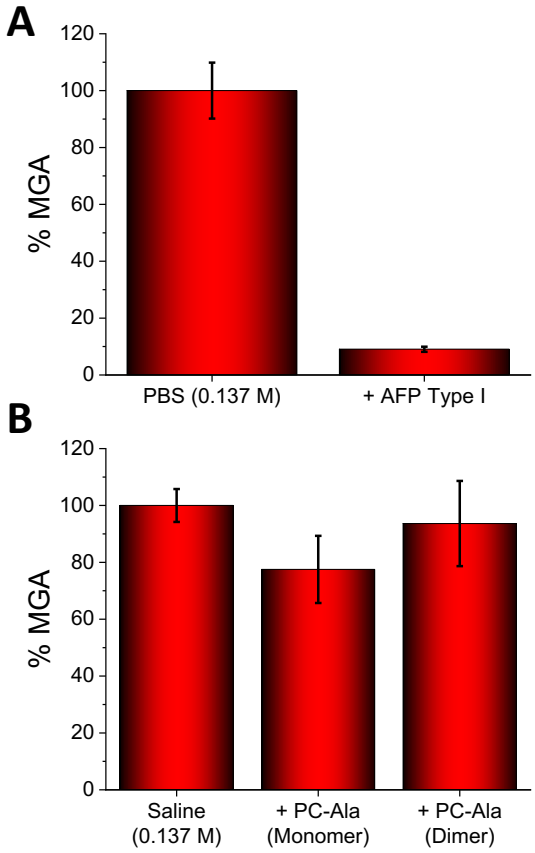

Figure 7. Ice recrystallization inhibition activity of controls. A) Recombinant Type AFP Type I (2 μg.mL^{-1}). B) PC-Ala photoconjugates (both at 3.5 mg.mL^{-1}) before and after irradiations. Error bars are +/- S.D from minimum of 3 repeats. % Mean Grain Area (MGA) of all the ice crystals in field of view is reported relative to the negative saline control

As a positive control, recombinant Type I antifreeze protein (Figure 7A and ESI) was shown to have significant IRI activity at very low concentration (~10% MGA at 2 μg.mL^{-1}) highlighting the remarkable potency of these proteins. The PC-Ala had essentially no activity (and was statistically similar) in both the monomeric and dimerised states at 3.5 mg.mL^{-1} showing >80% MGA at its upper limit (7B). This enabled us to rule out the anthracene-dilysine having any intrinsic effect on IRI as amphiphilic molecules can inhibit ice growth.[58,59,10]

The truncated antifreeze peptides of 22 and 11 residues (repeat sequence; TAANAAAAAA) had less IRI activity at their solubility limits of 0.9 and 1 mg.mL^{-1} compared to the full sequence AFP as would be expected, Figure 8. AFP_{11} showed essentially no activity as both the peptide, the anthracene conjugate and as the dimer, indicating that this 11 residue sequence is too short to induce any IRI. The AFP_{22} also had essentially no IRI activity. But, unexpectedly, the addition of the anthracene unit appeared to 'turn on activity' with an MGA of ~ 30 % at just 0.6 mg.mL^{-1}. This is an exciting result as it is the first example, to the best of our knowledge, of an AFP having its activity regulated by addition of an end group. For full length AFPs addition of fusion proteins (e.g. a large end-group) is a passive modification leading to no change in activity,[60] and the same is seen using double hydrophilic blocks of poly(vinyl alcohol).[61] This may offer a route to make minimal synthetic AFPs by modulation of the end groups, and will be studied in the future. Upon photo irradiation of PC-AFP_{22} there was only a small (negative) change in observed IRI activity which was not statistically significant. However this may indicate that further engineering could widen this activity gap between the monomeric and dimeric forms, allowing for enhanced photoswitchability. We have previously reported that changing the architecture of both AFPs and polymeric IRIs, from linear to nanoparticle lead to no change in activity which supports what is seen here.[62,63–65] . Importantly, despite the increase in molecular weight, the

head-to-head assembly of the peptides after dimerization may explain why there is no increase in activity, disrupting the symmetry of the monomeric isoform and its matching of the prismatic ice face.

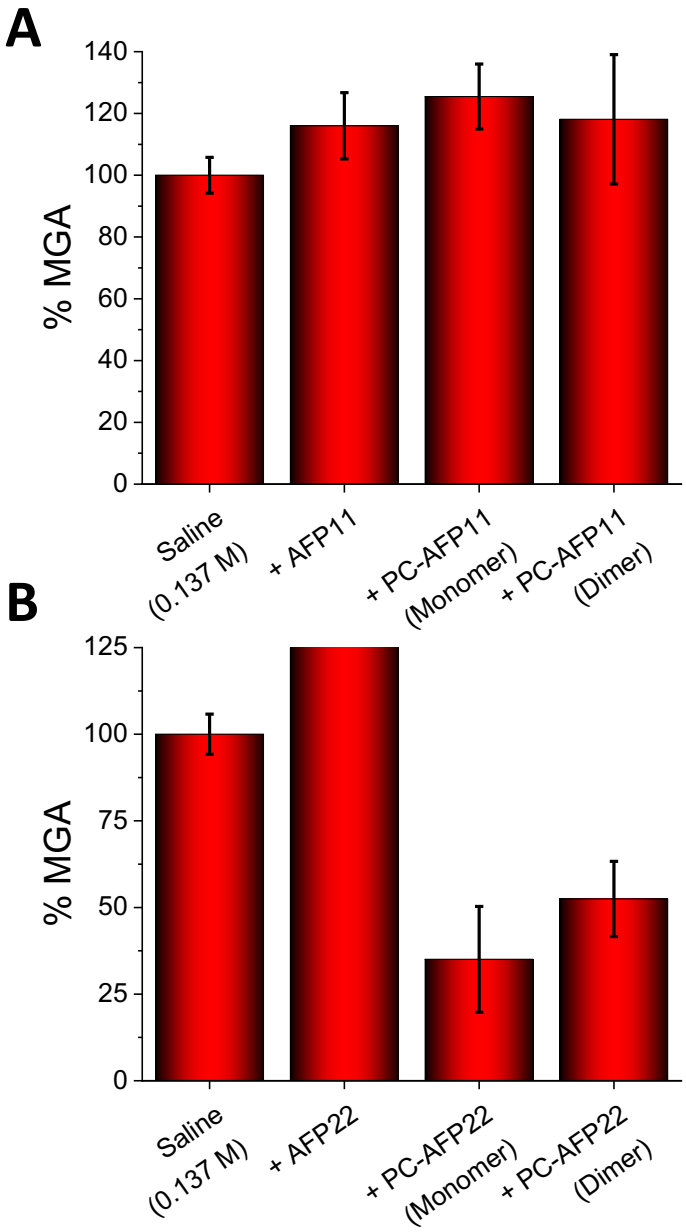

Figure 7. Ice recrystallization inhibition activity of AFP and conjugates. A) Native AFP_{11} and PC-AFP_{11} derivatives (1 $mg.mL^{-1}$); B) Free AFP_{22} (0.9 $mg.mL^{-1}$) and the PC-AFP_{22} derivatives

(at 0.6 mg.mL^{-1}). Error bars are +/- S.D from minimum of 3 repeats. % Mean Grain Area (MGA) reported relative to saline control.

Whilst the truncated AFPs used in this study are significantly less active than full length AFP, their activity is actually high compared to most reported synthetic mimics.[10,11] Figure 9 shows a comparison of the activity of the short peptides compared to poly(vinyl alcohol)$_{56}$, as reported by Congdon *et al.*[66], which is amongst the most active synthetic IRIs to-date.[48] We hypothesise that the increase in IRI activity is not simply due to the increased hydrophobicity, which has been shown by Ben et al. to be crucial in low-molecular weight IRIs.[67] We hypothesise this is due to the effect of the end-group to stabilise the secondary structure of the AFP$_{22}$, shown in the CD spectra in Figure 6. Figure 9B shows example cryo-micrographs of the effect of photo-dimerization on the activity of PC-AFP$_{22}$ highlighting the visible change in ice crystal size, even though the magnitude is too low for applications. Additionally we used wide angle x-ray scattering (WAXS) to probe the change in ice growth rates (this method enables 100's of crystals to be tested). In agreement with the 'splat' assay, there was a small difference in the rate of ice growth between the irradiated forms, but this gap is not large enough for any application (ESI). Nonetheless it does show that controlling peptide assembly offers a route to photo-control of IRI activity. Attempts to further characterize the material by SAXS (small angle x-ray scattering) did not lead to reliable data due to the low solubility of the material and hence further structural analyses were not possible. We also explored photo-dimerization of anthracene-terminated poly(vinyl alcohol)$_{11}$ as a polymeric equivalent. Similarly to the PC-AFP$_{22}$, the dimerization did not result in a significant change in activity (Supporting Information). This suggested that the spacer used may break the sequence required for extended ice-face binding, acting as a flexible junction, and hence being less active than linear PVA$_{22}$ would be expected to be. Consequently,

the AFP-dimer may also suffer from this junction preventing both blocks engaging with ice. This work help guide the future development of IRI's with spatio-temporal control over activity.

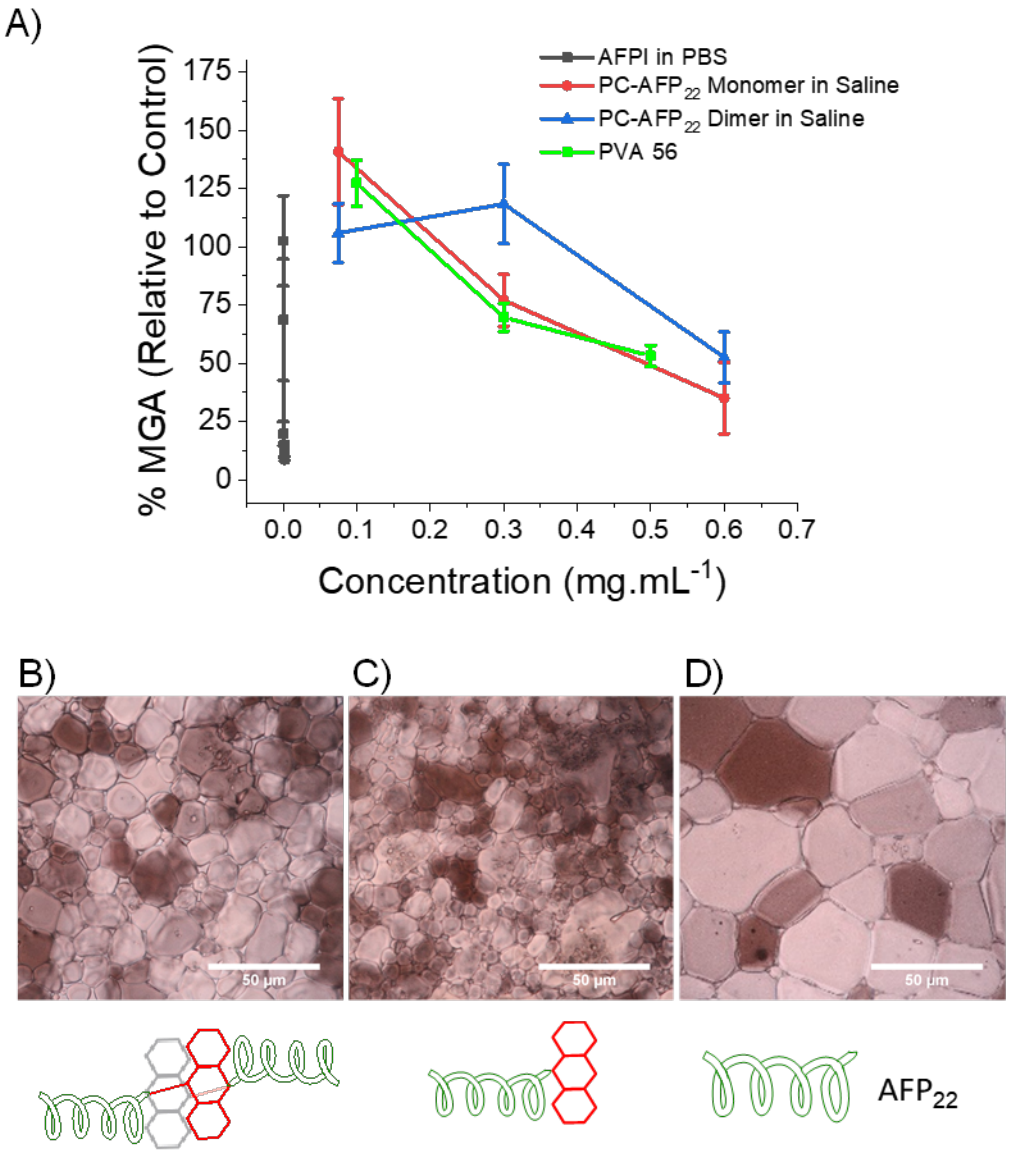

Figure 9. A) Ice recrystallization inhibition activity summary of peptides compared to full length AFP. Example cryomicrographs of ice wafers for the PC-AFP_{22} conjugate in B) dimer (0.6 $mg.mL^{-1}$); (C) and monomer (0.6 $mg.mL^{-1}$); (D), free AFP_{22} sequence (0.9 $mg.mL^{-1}$). Error bars are +/- S.D from minimum of 3 repeats. % Mean Grain Area (MGA) reported relative to saline control.

Conclusions

This work reports the synthesis and characterization of a panel of anthracene-conjugated peptides derived from the consensus repeat sequence of Type I antifreeze proteins. The synthetic route was optimised to include an additional di-lysine linker to ensure the conjugates were sufficiently water soluble, as the truncated peptides themselves are alanine-rich and display limited aqueous solubility. The truncated peptides alone were found to have no ice recrystallization inhibition activity at their solubility limit, as did the anthracene conjugate of the 11-amino acid peptide. However, the 22-mer was found to have a remarkable, and unexpected, increase in ice recrystallisation inhibition activity upon addition of the anthracene unit. This result was exciting as it shows that minimal peptides derived from AFP sequences (obtainable from solid phase synthesis rather than recombinant expression) may be useful IRIs, with their activity modulated by addition of non-peptide chain-end functionality. We hypothesise that the enhancement seen was due to the anthracene stabilising the secondary structure in the short peptide, supported by circular dichroism measurements, rather than aggregation. The overall activity of this adduct was comparable to poly(vinyl alcohol) which is the most active polymeric inhibitor known, highlighting the activity gain by this end-group modification. The anthracene conjugates were also explored for their photo-switchability under UV-light. Using UV-Vis spectroscopy, CD spectroscopy and HPLC photo-dimerization was shown to be very efficient with close to 100 % dimerization occurring. The ice recrystallisation inhibition activity before and after irradiation was very similar with only a small change in grain size, suggesting the dimerization process is partially tolerated but does not enhance activity. These results will help guide the development of externally-controllable ice growth modifiers as well as inspire a new range of minimal AFP mimetic peptides for application in biomedicine.

Supporting Information

Additional experimental information, assays, characterization data, and synthetic procedures can be found in the electronic supporting information (ESI) associated with this manuscript. This material is available free of charge *via* the internet at http://pubs.acs.org.

The research data supporting this publication can be found at http://wrap.warwick.ac.uk.

AUTHOR INFORMATION

Corresponding Author

*E-mail: M.I.Gibson@warwick.ac.uk (M.I. Gibson)

Author Contributions

The manuscript was written through contributions of all authors. All authors have given approval to the final version of the manuscript.

Notes

The research data supporting this publication can be found at http://wrap.warwick.ac.uk.

ACKNOWLEDGMENT

MIG holds an ERC starting grant (CRYOMAT 638661) and ERC PoC grant (CRYOSTEM 789182). Thanks go to Dr. Muhammad Hassan for the provision of AFP Type I protein data, and Dr. Steven Huband for WAXS and SAXS studies, respectively. Thanks also go to Prof. Alison Rodger for CD advice.

REFERENCES

(1) Guo, S.; Stevens, C. A.; Vance, T. D. R.; Olijve, L. L. C.; Graham, L. A.; Campbell, R. L.; Yazdi, S. R.; Escobedo, C.; Bar-Dolev, M.; Yashunsky, V.; Braslavsky, I.; Langelaan, D. N.; Smith, S. P.; Allingham, J. S.; Voets, I. K.; Davies, P. L. Structure of a 1.5-MDa Adhesin That Binds Its Antarctic Bacterium to Diatoms and Ice. *Sci. Adv.* **2017**, *3* (8), e1701440.

(2) Davies, P. L. Ice-Binding Proteins: A Remarkable Diversity of Structures for Stopping and Starting Ice Growth. *Trends Biochem. Sci.* **2014**, *39* (11), 548–555.

(3) Harding, M. M.; Anderberg, P. I.; Haymet, A. D. J. "Antifreeze" Glycoproteins from Polar Fish. *Eur. J. Biochem.* **2003**, *270* (7), 1381–1392.

(4) Fletcher, G. L.; Idler, D. R.; Vaisius, A.; Hew, C. L. Hormonal Regulation of Antifreeze Protein Gene Expression in Winter Flounder. *Fish Physiol. Biochem.* **1989**, *7* (1–6), 387–393.

(5) Yiu, W. K.; Basco, M. T.; Aruny, J. E.; Cheng, S. W. K.; Sumpio, B. E. Cryosurgery: A Review. *Int. J. Angiol.* **2007**, *16* (1), 1–6.

(6) Fowler, A.; Toner, M. Cryo-Injury and Biopreservation. *Ann. N. Y. Acad. Sci.* **2005**, *1066*, 119–135.

(7) Whittaker, D. K. Mechanisms of Tissue Destruction Following Cryosurgery. *Ann. R. Coll. Surg. Engl.* **1984**, *66* (5), 313–318.

(8) Prohaska, J.; Badri, T. *Cryotherapy*; StatPearls Publishing, 2018.

(9) Voets, I. K. From Ice-Binding Proteins to Bio-Inspired Antifreeze Materials. *Soft Matter* **2017**, *13* (28), 4808–4823.

(10) Biggs, C. I.; Stubbs, C.; Graham, B.; Fayter, A. E. R.; Hasan, M.; Gibson, M. I. Mimicking the Ice Recrystallization Activity of Biological Antifreezes. When Is a New Polymer "Active"? *Macromol. Biosci.* **2019**, *19* (7), 1900082.

(11) Biggs, C. I.; Bailey, T. L.; Ben Graham; Stubbs, C.; Fayter, A.; Gibson, M. I. Polymer Mimics of Biomacromolecular Antifreezes. *Nat. Commun.* **2017**, *8* (1), 1546.

(12) Balcerzak, A. K.; Capicciotti, C. J.; Briard, J. G.; Ben, R. N. Designing Ice Recrystallization Inhibitors : From Antifreeze (Glyco) Proteins to Small Molecules. *RSC Adv.* **2014**, *4*, 42682–42696.

(13) Carpenter, J. F.; Hansen, T. N. Antifreeze Protein Modulates Cell Survival during Cryopreservation: Mediation through Influence on Ice Crystal Growth. *Proc. Natl. Acad. Sci. U. S. A.* **1992**, *89* (19), 8953–8957.

(14) Deller, R. C.; Vatish, M.; Mitchell, D. A.; Gibson, M. I. Synthetic Polymers Enable Non-Vitreous Cellular Cryopreservation by Reducing Ice Crystal Growth during Thawing. *Nat. Commun.* **2014**, *5*, 3244.

(15) Capicciotti, C. J.; Kurach, J. D. R.; Turner, T. R.; Mancini, R. S.; Acker, J. P.; Ben, R. N. Small Molecule Ice Recrystallization Inhibitors Enable Freezing of Human Red Blood Cells with Reduced Glycerol Concentrations. *Sci. Rep.* **2015**, *5*, 9692.

(16) Geng, H.; Liu, X.; Shi, G.; Bai, G.; Ma, J.; Chen, J.; Wu, Z.; Song, Y.; Fang, H.; Wang, J.

Graphene Oxide Restricts Growth and Recrystallization of Ice Crystals Communications Angewandte. *Angew. Chem. Int. Ed.* **2017**, *56* (4), 997–1001.

(17) Matsumoto, S.; Matsusita, M.; Morita, T.; Kamachi, H.; Tsukiyama, S.; Furukawa, Y.; Koshida, S.; Tachibana, Y.; Nishimura, S. I.; Todo, S. Effects of Synthetic Antifreeze Glycoprotein Analogue on Islet Cell Survival and Function during Cryopreservation. *Cryobiology* **2006**, *52* (1), 90–98.

(18) Matsumura, K.; Bae, J. Y.; Kim, H. H.; Hyon, S. H. Effective Vitrification of Human Induced Pluripotent Stem Cells Using Carboxylated Poly-l-Lysine. *Cryobiology* **2011**, *63* (2), 76–83.

(19) Graham, B.; Bailey, T. L.; Healey, J. R. J.; Marcellini, M.; Deville, S.; Gibson, M. I. Polyproline Is a Minimal Antifreeze Protein Mimetic and Enhances the Cryopreservation of Cell Monolayers. *Angew. Chem. Int. Ed.* **2017**, *56*, 15941–15944.

(20) Deller, R. C.; Pessin, J. E.; Vatish, M.; Mitchell, D. A.; Gibson, M. I. Enhanced Non-Vitreous Cryopreservation of Immortalized and Primary Cells by Ice-Growth Inhibiting Polymers. *Biomater. Sci.* **2016**, *47*, 935–945.

(21) Chaytor, J. L.; Tokarew, J. M.; Wu, L. K.; Leclre, M.; Tam, R. Y.; Capicciotti, C. J.; Guolla, L.; Von Moos, E.; Findlay, C. S.; Allan, D. S.; Ben, R. N. Inhibiting Ice Recrystallization and Optimization of Cell Viability after Cryopreservation. *Glycobiology* **2012**, *22* (1), 123–133.

(22) Koushafar, H.; Pham, L.; Lee, C.; Rubinsky, B. Chemical Adjuvant Cryosurgery with Antifreeze Proteins. *J. Surg. Oncol.* **1997**, *66* (2), 114–121.

(23) Kloxin, A. M.; Tibbitt, M. W.; Kasko, A. M.; Fairbairn, J. A.; Anseth, K. S. Tunable Hydrogels for External Manipulation of Cellular Microenvironments through Controlled Photodegradation. *Adv. Mater.* **2010**, *22* (1), 61–66.

(24) Brown, T. E.; Anseth, K. S. Spatiotemporal Hydrogel Biomaterials for Regenerative Medicine. *Chem. Soc. Rev.* **2017**, *46* (21), 6532–6552.

(25) Fors, B. P.; Hawker, C. J. Control of a Living Radical Polymerization of Methacrylates by Light. *Angew. Chemie - Int. Ed.* **2012**, *51* (35), 8850–8853.

(26) Fu, C.; Huang, Z.; Hawker, C. J.; Moad, G.; Xu, J.; Boyer, C. RAFT-Mediated, Visible Light-Initiated Single Unit Monomer Insertion and Its Application in the Synthesis of Sequence-Defined Polymers. *Polym. Chem.* **2017**, *8* (32), 4637–4643.

(27) Wenn, B.; Conradi, M.; Carreiras, A. D.; Haddleton, D. M.; Junkers, T. Photo-Induced Copper-Mediated Polymerization of Methyl Acrylate in Continuous Flow Reactors. *Polym. Chem.* **2014**, *5* (8), 3053–3060.

(28) Yamada, M.; Suzuki, Y.; Nagasaki, S. C.; Okuno, H.; Imayoshi, I. Light Control of the Tet Gene Expression System in Mammalian Cells. *Cell Rep.* **2018**, *25* (2), 487–500.

(29) Reis, S. A.; Ghosh, B.; Hendricks, J. A.; Szantai-Kis, D. M.; Törk, L.; Ross, K. N.; Lamb, J.; Read-Button, W.; Zheng, B.; Wang, H.; Salthouse, C.; Haggarty, S. J.; Mazitschek, R. Light-Controlled Modulation of Gene Expression by Chemical Optoepigenetic Probes. *Nat. Chem. Biol.* **2016**, *12* (5), 317–323.

(30) Adam, M. K.; Hu, Y.; Poisson, J. S.; Pottage, M. J.; Ben, R. N.; Wilkinson, B. L.

Photoswitchable Carbohydrate-Based Fluorosurfactants as Tuneable Ice Recrystallization Inhibitors. *Carbohydr. Res.* **2017**, *439*, 1–8.

(31) Adam, M. K.; Poisson, J. S.; Hu, Y.; Prasannakumar, G.; Pottage, M. J.; Ben, R. N.; Wilkinson, B. L. Carbohydrate-Based Surfactants as Photocontrollable Inhibitors of Ice Recrystallization. *RSC Adv.* **2016**, *6* (45), 39240–39244.

(32) Müller, A.; Kobarg, H.; Chandrasekaran, V.; Gronow, J.; Sönnichsen, F. D.; Lindhorst, T. K. Synthesis of Bifunctional Azobenzene Glycoconjugates for Cysteine-Based Photosensitive Cross-Linking with Bioactive Peptides. *Chem. - A Eur. J.* **2015**, *21* (39), 13723–13731.

(33) Phillips, D. J.; Congdon, T. R.; Gibson, M. I. Activation of Ice Recrystallization Inhibition Activity of Poly(Vinyl Alcohol) Using a Supramolecular Trigger. *Polym. Chem.* **2016**, *7* (9), 1701–1704.

(34) Beharry, A. A.; Woolley, G. A. Azobenzene Photoswitches for Biomolecules. *Chem. Soc. Rev.* **2011**, *40* (8), 4422–4437.

(35) Garner, J.; Harding, M. M. Design and Synthesis of A-Helical Peptides and Mimetics. *Org. Biomol. Chem.* **2007**, *5* (22), 3577–3585.

(36) Filpponen, I.; Sadeghifar, H.; Argyropoulos, D. S. Photoresponsive Cellulose Nanocrystals. *Nanomater. Nanotechnol.* **2011**, *1*, 7.

(37) Aemissegger, A.; Kräutler, V.; Van Gunsteren, W. F.; Hilvert, D. A Photoinducible β-Hairpin. *J. Am. Chem. Soc.* **2005**, *127* (9), 2929–2936.

(38) Bartels, E.; Wassermann, N. H.; Erlanger, B. F. Photochromic Activators of the Acetylcholine Receptor. *Proc. Natl. Acad. Sci.* **2006**, *68* (8), 1820–1823.

(39) Bullen, G. A.; Tucker, J. H. R.; Peacock, A. F. A. Exploiting Anthracene Photodimerization within Peptides: Light Induced Sequence-Selective DNA Binding. *Chem. Commun.* **2015**, *51* (38), 8130–8133.

(40) Hasegawa, M.; Suzuki, A.; Matsumura, S.; Toshima, K. Molecular Design, Chemical Synthesis, and Evaluation of Novel Anthracene Derivatives as a New Family of Protein Photocleavers. *Sci. Technol. Adv. Mater.* **2006**, *7* (2), 169–174.

(41) Sun, H.; Kabb, C. P.; Dai, Y.; Hill, M. R.; Ghiviriga, I.; Bapat, A. P.; Sumerlin, B. S. Macromolecular Metamorphosis via Stimulusinduced Transformations of Polymer Architecture. *Nat. Chem.* **2017**, *9* (8), 817–823.

(42) Tucker, J. H. R.; Giordano, L.; Zhao, Z.; Manchester, J.; Bassani, D. M.; Vyle, J. S.; Duprey, J.-L. H. A. Photocontrolled Binding and Binding-Controlled Photochromism within Anthracene-Modified DNA. *J. Am. Chem. Soc.* **2012**, *134* (26), 10791–10794.

(43) Bouas-Laurent, H.; Castellan, A.; Desvergne, J. P.; Lapouyade, R. Photodimerization of Anthracenes in Fluid Solution: Structural Aspects. *Chem. Soc. Rev.* **2000**, *29* (1), 43–55.

(44) Maturi, M. M.; Fukuhara, G.; Tanaka, K.; Kawanami, Y.; Mori, T.; Inoue, Y.; Bach, T. Enantioselective [4+4] Photodimerization of Anthracene-2,6-Dicarboxylic Acid Mediated by a C2-Symmetric Chiral Template. *Chem. Commun.* **2016**, *52* (5), 1032–1035.

(45) Dawn, A.; Fujita, N.; Haraguchi, S.; Sada, K.; Shinkai, S. An Organogel System Can

Control the Stereochemical Course of Anthracene Photodimerization. *Chem. Commun.* **2009**, *0* (16), 2100–2102.

(46) Houston, M. E.; Chao, H.; Hodges, R. S.; Sykes, B. D.; Kay, C. M.; Sönnichsen, F. D.; Loewen, M. C.; DAvies, P. L. Binding of an Oligopeptide to a Specific Plane of Ice. *J. Biol. Chem.* **1998**, *273* (19), 11714–11718.

(47) Urbańczyk, M.; Góra, J.; Latajka, R.; Sewald, N. Antifreeze Glycopeptides: From Structure and Activity Studies to Current Approaches in Chemical Synthesis. *Amino Acids* **2017**, *49* (2), 209–222.

(48) Congdon, T.; Notman, R.; Gibson, M. I. Antifreeze (Glyco)Protein Mimetic Behavior of Poly(Vinyl Alcohol): Detailed Structure Ice Recrystallization Inhibition Activity Study. *Biomacromolecules* **2013**, *14* (5), 1578–1586.

(49) Mahatabuddin, S.; Hanada, Y.; Nishimiya, Y.; Miura, A.; Kondo, H.; Davies, P. L.; Tsuda, S. Concentration-Dependent Oligomerization of an Alpha-Helical Antifreeze Polypeptide Makes It Hyperactive. *Sci. Rep.* **2017**, *7*, 42501.

(50) Hakim, A.; Nguyen, J. B.; Basu, K.; Zhu, D. F.; Thakral, D.; Davies, P. L.; Isaacs, F. J.; Modis, Y.; Meng, W. Crystal Structure of an Insect Antifreeze Protein and Its Implications for Ice Binding. *J. Biol. Chem.* **2013**, *288* (17), 12295–12304.

(51) Xue, B.; Zhao, L.; Qin, X.; Qin, M.; Lai, J.; Huang, W.; Lei, H.; Wang, J.; Wang, W.; Li, Y.; Cao, Y. Bioinspired Ice Growth Inhibitors Based on Self-Assembling Peptides. *ACS Macro Lett.* **2019**, *8* (10), 1383–1390.

(52) Kamei, Y.; Sudo, A.; Nishida, H.; Kikukawa, K.; Endo, T. Synthesis of Polypeptides from Activated Urethane Derivatives of α-Amino Acids. *J. Polym. Sci. Part A Polym. Chem.* **2008**, *46* (7), 2525–2535.

(53) Knight, C. A.; Wen, D.; Laursen, R. A. Nonequilibrium Antifreeze Peptides and the Recrystallization of Ice. *Cryobiology* **1995**, *32* (1), 23–34.

(54) Wei, H.; Wang, Q.; Cheng, H.; Zhang, X.; Kan, L.; Li, B.; Ma, N. Anthracene Dimer Crosslinked Polyurethanes as Mechanoluminescent Polymeric Materials. *New J. Chem.* **2019**, *43* (6), 2658–2664.

(55) Kihara, H.; Yoshida, M. Reversible Phase Change of New Anthracene Compounds Triggered by the Action of Light and Heat. In *IOP Conference Series: Materials Science and Engineering*; IOP Publishing, 2014; Vol. 54, p 012020.

(56) Mu, Y.; Tang, B.; Yu, M. Length-Dependent β-Sheet Growth Mechanisms of Polyalanine Peptides in Water and on Hydrophobic Surfaces. *Phys. Rev. E - Stat. Nonlinear, Soft Matter Phys.* **2014**, *89* (3), 032711.

(57) Wakai, A.; Fukasawa, H.; Yang, C.; Mori, T.; Inoue, Y. Theoretical and Experimental Investigations of Circular Dichroism and Absolute Configuration Determination of Chiral Anthracene Photodimers. *J. Am. Chem. Soc.* **2012**, *134* (10), 4990–4997.

(58) Adam, M. K.; Jarrett-Wilkins, C.; Beards, M.; Staykov, E.; MacFarlane, L. R.; Bell, T. D. M.; Matthews, J. M.; Manners, I.; Faul, C. F. J.; Moens, P. D. J.; Ben, R. N.; Wilkinson, B. L. 1D Self-Assembly and Ice Recrystallization Inhibition Activity of Antifreeze Glycopeptide-Functionalized Perylene Bisimides. *Chem. - A Eur. J.* **2018**, *24* (31), 7834–

7839.

(59) Mitchell, D. E.; Clarkson, G.; Fox, D. J.; Vipond, R. A.; Scott, P.; Gibson, M. I. Antifreeze Protein Mimetic Metallohelices with Potent Ice Recrystallization Inhibition Activity. *J. Am. Chem. Soc.* **2017**, *139* (29), 9835–9838.

(60) DeLuca, C. I.; Comley, R.; Davies, P. L. Antifreeze Proteins Bind Independently to Ice. *Biophys. J.* **1998**, *74* (3), 1502–1508.

(61) Congdon, T. R.; Notman, R.; Gibson, M. I. Influence of Block Copolymerization on the Antifreeze Protein Mimetic Ice Recrystallization Inhibition Activity of Poly(Vinyl Alcohol). *Biomacromolecules* **2016**, *17* (9), 3033–3039.

(62) Wilkins, L. E.; Hasan, M.; Fayter, A. E. R.; Biggs, C.; Walker, M.; Gibson, M. I. Site-Specific Conjugation of Antifreeze Proteins onto Polymer-Stabilized Nanoparticles. *Polym. Chem.* **2019**, *10*, 2986–2990.

(63) Stevens, C. A.; Drori, R.; Zalis, S.; Braslavsky, I.; Davies, P. L. Dendrimer-Linked Antifreeze Proteins Have Superior Activity and Thermal Recovery. *Bioconjug. Chem.* **2015**, *26* (9), 1908–1915.

(64) Stubbs, C.; Wilkins, L. E.; Fayter, A. E. R.; Walker, M.; Gibson, M. I. Multivalent Presentation of Ice Recrystallization Inhibiting Polymers on Nanoparticles Retains Activity. *Langmuir* **2019**, *35* (23), 7347–7353.

(65) Olijve, L. L. C.; Hendrix, M. M. R. M.; Voets, I. K. Influence of Polymer Chain Architecture of Poly(Vinyl Alcohol) on the Inhibition of Ice Recrystallization. *Macromol.*

Chem. Phys. **2016**, *217* (8), 951–958.

(66) Congdon, T.; Dean, B. T.; Kasperczak-Wright, J.; Biggs, C. I.; Notman, R.; Gibson, M. I. Probing the Biomimetic Ice Nucleation Inhibition Activity of Poly(Vinyl Alcohol) and Comparison to Synthetic and Biological Polymers. *Biomacromolecules* **2015**, *16* (9), 2820–2826.

(67) Capicciotti, C. J.; Leclere, M.; Perras, F. A.; Bryce, D. L.; Paulin, H.; Harden, J.; Liu, Y.; Ben, R. N. Potent Inhibition of Ice Recrystallization by Low Molecular Weight Carbohydrate-Based Surfactants and Hydrogelators. *Chem. Sci.* **2012**, *3* (5), 1408–1416.